An intrinsically three dimensional fractal

M. Fernández Guasti

Lab. de Óptica Cuántica, Depto. de Física,
Universidad A. Metropolitana - Iztapalapa,
09340 México D.F., Ap. postal. 55-534, MEXICO
e-mail: mfg@xanum.uam.mx, url: http://luz.izt.uam.mx

Abstract

The quadratic iteration is mapped using a non distributive real scator algebra in three dimensions. The bound set, labeled $\mathbf{c2i0}\mathbb{E}_+^2$, has a rich fractal like boundary. Periodic points on the scalar axis are necessarily surrounded by off axis divergent magnitude surfaces. The three dimensional set exhibits self-similar 3D copies of the elementary fractal along the negative scalar axis. Nonetheless, the two dimensional projection becomes identical to the non-fractal quadratic iteration produced with hyperbolic numbers. Two and three dimensional renderings are presented to explore some of the features of the $\mathbf{c2i0}\mathbb{E}_+^2$ set. New algorithms are needed to visualize the intricacies of these higher dimensional fractal sets.

Keywords: Fractals; Hyper-complex numbers; 3D hyperbolic numbers; Real scators; Quadratic iteration; Mandelbrot set, Discrete dynamical systems.

1. Introduction

Two dimensional fractal structures have often been extended to higher dimensions. For example: Sierpinski triangles are extended to three dimensional tetrahedrons that produce square based pyramids; Sphere inversion fractals as a generalization of circle inversion [Leys, 2005]; Mandelbulb [Aron, 2009], Mandelbox and several other approaches to generalizations of fractals in the complex plane to three or four dimensions. However, the generalization does not always produce a higher dimensional fractal structure. For example, quaternion quadratic iterations in parameter space produce solids of revolution with an M-set section. The visualization of fractal geometry, even in two dimensions, is a rich subject [Blackledge, 2002]. Visualization of three dimensional structures is even more complicated and requires complex and cpu-time consuming algorithms [Dodge et al., 2008].

It is not common practice to proceed the other way around. Namely, to produce a three dimensional fractal structure and thereafter obtain two dimensional projections of these objects. In the present approach, the three dimensional product and addition operations required to produce a quadratic mapping are introduced. The iteration of the quadratic function with three variables is compared with an appropriate order parameter. The outcome is a bound set with a rather intricate boundary that is rendered with an ad hoc 3D fractal visualization software. It comes as a surprise that a three dimensional confined set, produced with real scator algebra, exhibits fractal features whereas the two dimensional projection does not. This projection is isomorphic to hyperbolic or perplex numbers. Under the quadratic iteration, it is known that hyperbolic numbers produce a square bound set with a smooth boundary that does not show fractal features. In section 2, real scator algebra in 1+2 dimensions is reviewed. The quadratic iteration with this number system is presented in section 3. The divergent magnitude surfaces present in the vicinity of periodic points is established in subsection 3.1. The dual numbers limit and 2D projections in the s, x plane are presented in section 4.

2. Hyperbolic scators

Real scator elements in 1+2 dimensions can be written in terms of three real numbers

$$\overset{o}{\varphi} = (F_0; F_1, F_2) \,, \ F_j \in \mathbb{R}.$$

The first component stands on a different footing from the rest. To stress this fact, it is separated by a semi-colon from the other components. It is labeled with subindex zero and named the scalar component. Subsequent components, separated by commas, stand on an equal footing. They are named the director components because, as we shall see, they possess a direction. Scator elements are represented with an oval placed overhead[1]. The *addition* operation for scators $\overset{o}{\alpha}, \overset{o}{\beta}$ is defined component-wise

$$\overset{o}{\alpha} + \overset{o}{\beta} \equiv (A_0; A_1, A_2) + (B_0; B_1, B_2) = (A_0 + B_0; A_1 + B_1, A_2 + B_2) \,.$$

The scator set forms a commutative group under the addition operation. The *product* operation for scators, $\overset{o}{\alpha} = (A_0; A_1, A_2)$ and $\overset{o}{\beta} = (B_0; B_1, B_2)$ is defined by $\overset{o}{\gamma} = \overset{o}{\alpha}\overset{o}{\beta} \equiv (G_0; G_1, G_2)$, where the scalar component of the product is

$$G_0 = A_0 B_0 + A_1 B_1 + A_2 B_2 + \frac{A_1 B_1 A_2 B_2}{A_0 B_0} \tag{2.1a}$$

---

[1] \overset{o} in LaTeX lore

2

and the director components of the product are

$$G_1 = B_0 A_1 + A_0 B_1 + \frac{A_1 A_2 B_2}{A_0} + \frac{A_2 B_1 B_2}{B_0}, \tag{2.1b}$$

$$G_2 = B_0 A_2 + A_0 B_2 + \frac{A_1 A_2 B_1}{A_0} + \frac{A_1 B_1 B_2}{B_0}. \tag{2.1c}$$

In order to have a product without divergent components, it is necessary that the scalar components of the factors are different from zero if two or more director components are different from zero. The subspace $\mathbb{E}_+^2 \subset \mathbb{R}^3$, where the product components are finite is

$$\left(\mathbb{E}_+^2, \cdot\right) = \left\{ \overset{o}{\alpha}, \overset{o}{\beta} \in \mathbb{E}_+^2 : A_0, B_0 \neq 0 \text{ if } A_1 B_1, A_2 B_2 \neq 0 \right\}. \tag{2.2}$$

The plus subindex in $\mathbb{E}_+^2$ recalls that the product of a single director component times itself is equal to $+1$; The superindex plus one is equal to the number of dimensions. The set that includes points at infinity, following the extended complex plane notation, is labeled as $\bar{\mathbb{E}}_+^2$. Hyperbolic 1+2 dimensional scators form a commutative group under the product operation provided that non invertible elements and divisors of zero are excluded [Fernández-Guasti and Zaldivar, 2013]. The subspace $\mathbb{E}_{+g}^2$, where the product forms a commutative group is

$$\left(\mathbb{E}_{+g}^2, \cdot\right) = \left\{ \overset{o}{\alpha}, \overset{o}{\beta} \in \left(\mathbb{E}_+^2, \cdot\right) : \overset{o}{\alpha}, \overset{o}{\beta} \neq 0, A_0 \neq A_k, B_0 \neq B_k, \frac{A_k B_k}{A_0 B_0} \neq -1, k = 1, 2 \right\}. \tag{2.3}$$

The square of a scator is obtained from the product definition (2.1a)-(2.1c) between two equal scators $\overset{o}{\beta} = \overset{o}{\alpha}$. Let $A_0 = B_0 = s$, $A_1 = B_1 = x$ and $A_2 = B_2 = y$. The square of the scator $\overset{o}{\alpha} = (s; x, y)$ is then $\overset{o}{\gamma} = \overset{o}{\alpha}^2 = (G_0; G_1, G_2)$ with

$$G_0 = s^2 + x^2 + y^2 + \frac{x^2 y^2}{s^2} \tag{2.4a}$$

and the director components of the product are

$$G_1 = 2sx + \frac{2xy^2}{s} = 2x\left(s + \frac{y^2}{s}\right) \tag{2.4b}$$

$$G_2 = 2sy + \frac{2yx^2}{s} = 2y\left(s + \frac{x^2}{s}\right). \tag{2.4c}$$

The square of the magnitude of a scator $\left\|\overset{o}{\varphi}\right\|^2$ for a scator $\overset{o}{\varphi} = (F_0; F_1, F_2)$ is defined by the product of a scator times its conjugate

$$\left\|\overset{o}{\varphi}\right\|^2 = \overset{o}{\varphi}\overset{o}{\varphi}{}^* = \left(F_0^2 - F_1^2 - F_2^2 + \frac{F_1^2 F_2^2}{F_0^2}; 0, 0\right), \tag{2.5}$$

3

where the scator conjugate is $\overset{o}{\varphi}{}^{*} = (F_0; -F_1, -F_2)$. If condition (2.3) is fulfilled, the scator product of the norm is equal to the norm of the scator products. The scator norm product identity can be used to derive Lagrange's identity as well as other series identities [Fernández-Guasti, 2012]. The subspace $\mathbb{E}_+^2$ where the product components are finite, from (2.2), requires that $s \neq 0$ if $x \neq 0$ and $y \neq 0$. If s becomes very small while x, y are both different from zero, the magnitude of the scator becomes very large. There is a set of points on the x, y plane, in the vicinity of $s = 0$, whose magnitude approaches infinity

$$\mathbf{R}_s = \left\{ (s; x, y) \in \bar{\mathbb{E}}_+^2 \, : \, x \neq 0, \; y \neq 0, \; \|(s; x, y)\| \underset{s \to 0}{\longrightarrow} \infty \right\}. \qquad (2.6)$$
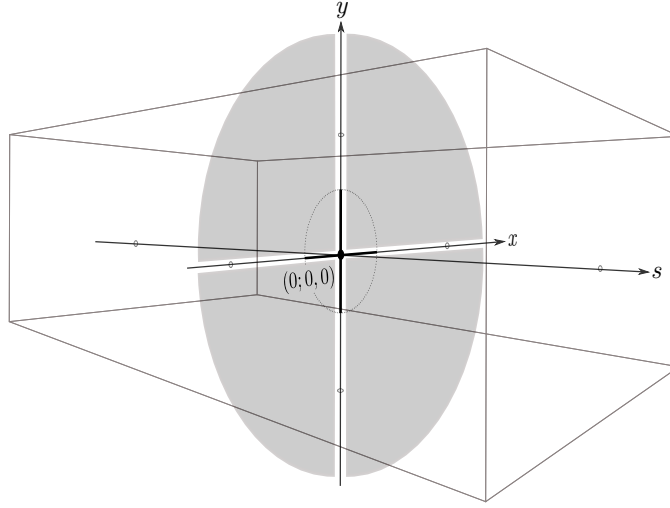
This set is depicted in figure 1.

Figure 1: Fixed point at the origin $0 = (0; 0, 0)$ and divergent magnitude plane (in gray) that covers the x, y plane except for the lines at $x = 0$ and $y = 0$. The darker cross in the x, y plane, whose length is $\pm 1/4$ in either axes, depicts the bound points on this plane under the quadratic iteration.

Therefore, the only points within the x, y plane that can be (but are not necessarily) bounded for $s = 0$ are those lying on the axis lines $x = 0$ or $y = 0$. We discuss this case in section 4.1.

Divisors of zero for invertible elements are obtained if the equalities $A_1 B_1 = -A_0 B_0$ and $A_2 B_2 = -A_0 B_0$ are fulfilled. For the square function (2.4a)-(2.4c), these conditions are never met, since for two identical scators, they imply that $x^2 = -s^2$ and $y^2 = -s^2$. However, since s, x, y are real, the condition is never attained. There are therefore no nilpotent elements in real scator algebra under the square operation.

The square of an invertible element is also an invertible element. To prove it, consider an arbitrary invertible element, that is, an element $\overset{o}{\alpha} = (A_0; A_1, A_2)$

4

where $A_0 \neq A_j$ for $j = 1, 2$. The quotient of the director over scalar for the square operation is

$$\frac{G_j}{G_0} = \frac{2\frac{A_j}{A_0}}{1 + \left(\frac{A_j}{A_0}\right)^2}.$$

If any of these two components is non-invertible, the quotient should be one, *i.e.* $\frac{G_j}{G_0} = 1$. Then $1 + \left(\frac{A_j}{A_0}\right)^2 = 2\frac{A_j}{A_0}$, that is $\left(\frac{A_j}{A_0} - 1\right)^2 = 0$. However, this condition can only be met if $A_0 = A_j$ but this equality contradicts the premise that the initial scator is invertible. The scalar component G_0 resultant from the square operation (2.4a), is always different from zero for any non-zero scator. Under these conditions, preimages $O^- \left(\overset{o}{\varphi}_0\right)$ can be obtained. For the square operation, the only non associative elements come from non invertible elements, that is, with $x^2 = s^2$ or $y^2 = s^2$. These elements lie on lines passing through the origin with $\pm \pi/4$ slope. In this case, inverse orbits cannot be obtained.

3. Iterated quadratic mapping

The family of quadratic maps $P_c : z \mapsto z^2 + c$ from $\bar{\mathbb{E}}_+^2$ to $\bar{\mathbb{E}}_+^2$ is given by

$$\overset{o}{\varphi} = \overset{o}{\varphi}_0^2 + \overset{o}{c},$$

where the variable $\overset{o}{\varphi}$ and the constant $\overset{o}{c}$ are now scator elements. The iterated function satisfies the recurrence relationship

$$\overset{o}{\varphi}_{n+1} = \overset{o}{\varphi}_n^2 + \overset{o}{c},$$

where the subindex stands for the iteration number. The Mandelbrot like set is obtained by fixing the initial point $\overset{o}{\varphi}_0 = (0; 0, 0)$ and varying the parameter $\overset{o}{c}$. Bounded points obtained with this procedure comprise the corresponding M-set in $\mathbb{E}_+^2$. There are an arbitrary number of intersections of the plane with a volume depending on the position and inclination of the plane. Therefore, there are infinitely many slices of the M-like set in $\mathbb{E}_+^2$ compared with the unique set obtained in $\mathbb{C}$. The *confined iteration* notation is used to allow for some orientation in several dimensions:

- **c2i** **c**onfined {**2**}quadratic **i**terations, (can be generalized to **cpi** for a p$^{\text{th}}$ power polynomial or p$\rightarrow func$ for other *func*tion's mappings)

- followed by **0** if the initial value of the variable is set to zero as it happens in parameter space

- followed by the number set: $\mathbb{R}$ real, $\mathbb{C}$ complex, $\mathbb{H}$ hyperbolic, $\mathbb{E}_+^n$ real scator (in $1 + n$ dimensions), etc.

5

- followed, if required, by the plane $(D_0; D_1, D_2)$ that is being depicted.

According to this notation, the Mandelbrot set in the complex plane is labeled as the **c2i0**$\mathbb{C}$ set. It is not necessary to show explicitly the plane that is being depicted since it is inevitably the complex plane.
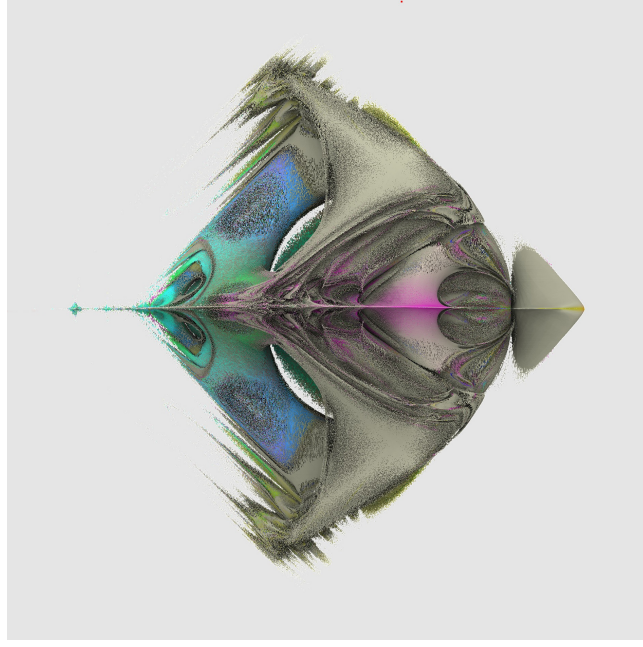

Figure 2: Three dimensional rendering of the **c2i0**$\mathbb{E}_+^2 (s; x, y)$ set viewed from the first director component, x axis. The abscissa corresponds to the real or scalar s axis $(-2.0 < s < 0.5)$, while the ordinate depicts the second director component, y axis $(-1.2 < y < 1.2)$. The x axis, comming out of the page, was scanned in the interval $-0.97 < x < 1.79$. 13 iterations per point were performed.

The M-like set for real scators in $1+2$ dimensions, labeled according to the *confined iteration* notation as **c2i0**$\mathbb{E}_+^2$ is given by

$$\mathbf{c2i0}\mathbb{E}_+^2 = \left\{ \overset{o}{c} \in \mathbb{E}_+^2 : \forall n \varepsilon \mathbb{N}, \| P^{\circ n} (0) \| \nrightarrow \infty \right\},$$

where $P : \overset{o}{\varphi} \mapsto \overset{o}{\varphi}^2 + \overset{o}{c}$, $P^{\circ n}$ denotes the *n-fold composition* $P^{\circ n} = P \circ P \circ \cdots \circ P$ of the function P with itself and the 0 argument in $P^{\circ n} (0)$ means that the function is initially evaluated at zero. Some remarks are required: i) the initial point in scator space $(0; 0, 0)$ is equal to the additive neutral $0 \in \mathbb{R}$; ii) The **c2i0**$\mathbb{E}_+^2$ set has been defined by the set of points whose magnitude remains bounded.

6

In complex algebra, it does not matter whether this condition is imposed on the magnitude or the real or imaginary parts. However, for real scators, these conditions are not equivalent just as it occurs for hyperbolic numbers [Pavlov et al., 2009]; iii) The M-set is often defined by the set of parameters c for which K_c, the Julia set, is connected [Douady and Hubbard, 1984]. This approach will be deferred until the K_c set is discussed in a forthcoming communication.

In order to evaluate the points in the set numerically, it is more appropriate to cast the divergence condition in terms of an upper bound b

$$\mathbf{c2i0}\mathbb{E}_+^2 = \left\{ \overset{o}{c} \in \mathbb{E}_+^2 : \forall n\varepsilon\mathbb{N}, \exists b\varepsilon\mathbb{R}, \|P^{\circ n}(0)\|^2 \leq b \right\}. \tag{3.1}$$

In real scator algebra, the magnitude squared is not positive definite. It is therefore necessary to perform the upper bound evaluation with the magnitude squared. For a different reason, namely, in order to avoid evaluating a CPU time consuming square root, it is customary to work with the square of the magnitude in the numerical code.

This set is no longer in two dimensions but in a three dimensional space. In figure 2, the image of a three dimensional rendering of the $\mathbf{c2i0}\mathbb{E}_+^2$ set is shown. This and subsequent three dimensional image representations were produced with P. Willenius rendering program [Willenius, 2013, v.2.0.1]. The number of points is 1.805×10^9, $(s = 1900) \times (x = 1900) \times (y = 500)$. Thirteen iterations are performed on each point. From these 1805 Mvoxels, only the points in the boundary are drawn. The colouring is due to the value of the components in the last iteration, the scalar, x and y directors values proportional to red, green and blue respectively (s_{13} {red}; x_{13} {green}, y_{13} {blue}). There is a bulge that looks smoother than the rest, spanning from 0 to 0.25 in the scalar axis (extreme right in figure 2). The confined set is squeezed at $s = 0$ where the bulge meets the complex structure on the left. The lack of bound points in the vicinity of the $s = 0$ plane is due to the set of repelling points $\mathbf{R}_s$ described in (2.6). The rendering suggests a series of onion like skins sewn at rather complex rims. Some of them resemble cardioid shapes while others do not seem to produce closed shapes. On the far left, there is a hint of a self-similar smaller version of the larger set. The entire fractal is inscribed in a diamond like shape, that as we shall see, corresponds to the two dimensional projection.
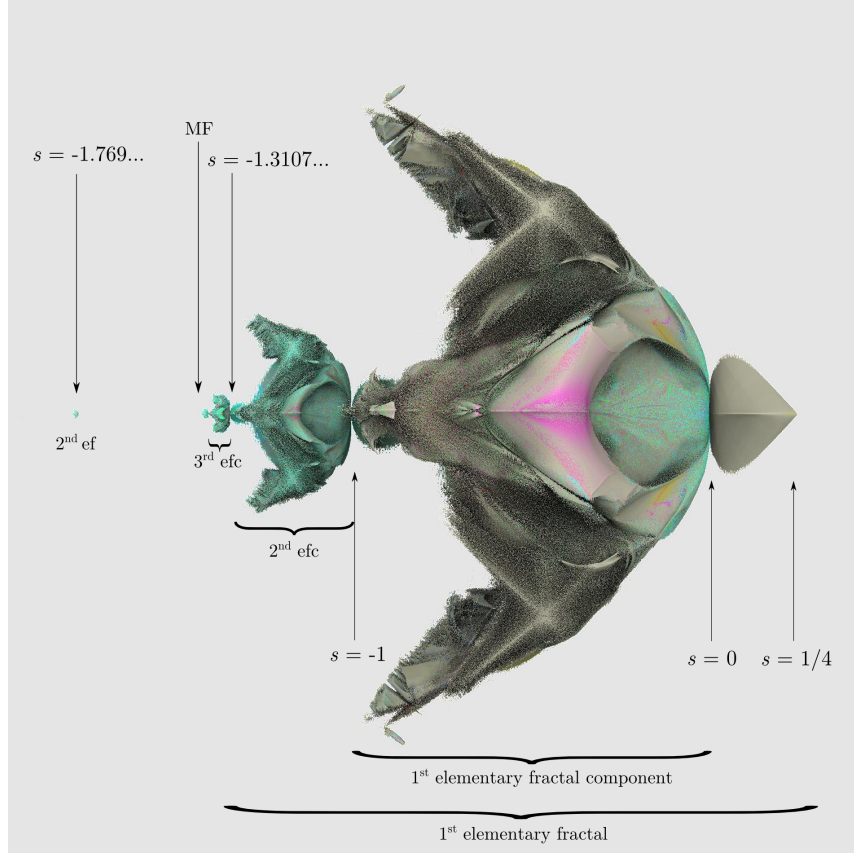
Figure 3: Three dimensional rendering of the **c2i0$\mathbb{E}_+^2$**$(s; x, y)$ set viewed from the first director component, x axis. 91 iterations per point were performed. The abscissa represents the real or scalar s axis, while the ordinate depicts the second director component, y axis.

The **c2i0$\mathbb{E}_+^2$** set is drawn again in figure 3. However, the number of iterations for each point has been increased ninefold from 13 (in figure 2) to 91. Since the bound set is defined for points where the magnitude remains bounded for an infinite number of iterations, it is expected that this latter rendering should be much closer to the actual set. This is true to some extent but it can be deceiving. Some regions in the set are extremely thin. When a few iterations are evaluated, these regions are partially 'caught' within the bound criterion. However, as the number of iterations increases, if the mesh points do not intersect with the thin bound regions they become lost. To retain them, a much finer mesh is required with the concomitant increase in the number of operations. To grasp some of the finer details an incredibly thin mesh will be required. A possibility in order to visualize these features is to have a variable thickness evaluation mesh and to introduce transparency for very thin features.

To describe the main features of the 3D set, let us borrow the concept of 'unit cell' or 'elementary cell' from crystallography. The simplest repeating atomic distribution or structure in a crystal is called a unit cell or elementary cell.

elementary fractal Any of the subsets that contains the whole fractal structure that is repeated.

n$^{\text{th}}$ elementary fractal The n$^{\text{th}}$ elementary fractal counted from large to small. The largest elementary fractal is labeled 1$^{\text{st}}$, the second largest 2$^{\text{nd}}$, etc.

In figure 3, the first elementary fractal (1$^{\text{st}}$ ef) spans from (s, x, y) roughly equal to $(-1.401$ to $0.25, \pm 1.125, \pm 1.125)$. The second elementary fractal can just be resolved in this figure and is located around $(-1.769, 0, 0)$. Several other order elementary fractals have been observed along the negative s axis between -2 and -1.401. In crystallography, the elementary cell repeats with the same size and orientation producing a lattice. In three dimensional fractals, the elementary fractal is repeated with the same shape but not necessarily with the same size nor orientation. In other words, the fractal lattice changes size and orientation. Furthermore, it need not be densely packed.

elementary fractal component A subset of the elementary fractal that is repeated within such structure. They are numbered from large to small.

There is an elementary fractal component contained within the volume given by $(-1$ to $0, \pm 1.125, \pm 1.125)$. The *first elementary fractal winged component* (1$^{\text{st}}$ *efwc*). A second *efwc* is roughly located within $(-1.3$ to $-1, \pm 0.3, \pm 0.3)$. These *efwc* are likely to be related to period doubling regions. This period doubling cascade seems to converge to the Myrberg-Feigenbaum (MF) point.

For $\overset{o}{c} = (s; x, y)$, the quadratic iteration recurrence relationship $\overset{o}{\varphi}_{n+1} = \overset{o}{\varphi}_n^2 + \overset{o}{c}$ for the scalar component is
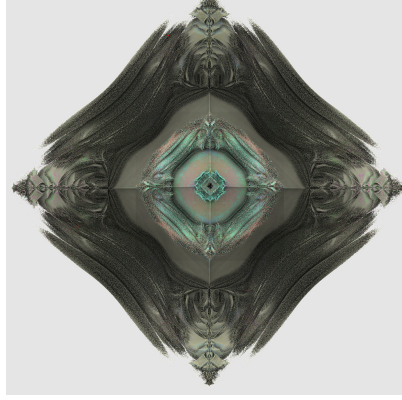
$$s_{n+1} = s_n^2 + x_n^2 + y_n^2 + \frac{x_n^2 y_n^2}{s_n^2} + s \qquad (3.2a)$$

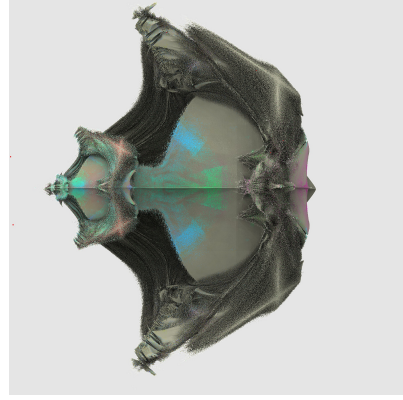and for the director components, the recurrence relationships are

$$x_{n+1} = 2s_n x_n + \frac{2x_n y_n^2}{s_n} + x, \qquad (3.2b)$$

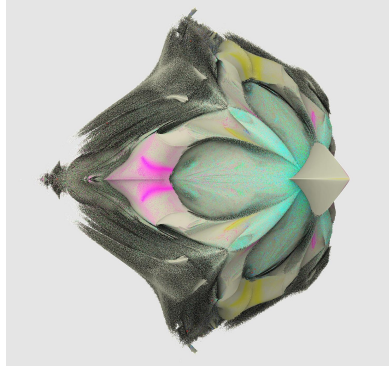$$y_{n+1} = 2s_n y_n + \frac{2y_n x_n^2}{s_n} + y. \qquad (3.2c)$$

Interchange of the x and y variables exchange the recurrence relationships for the director components. Thus, there should be symmetry with respect to the
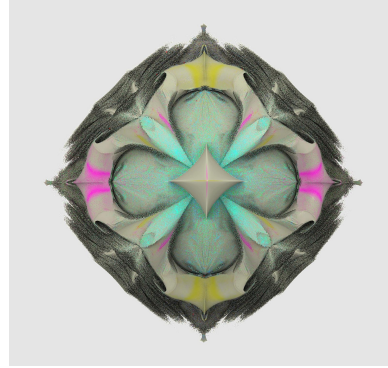
(a) View from $-s$ axis.

(b) View from $-\pi/4$ in (s, x) plane.

(c) View from $\pi/4$ in (s, x) plane.

(d) View from $+s$ axis. The x direction lies in the abscissa.

Figure 4: Different views of the **c2i0$\mathbb{E}_+^2$** set seen from the (s, x) plane. The ordinates correspond to the y direction in all figures.

$\pm\pi/4$ axes in the x, y plane. This symmetry is clearly seen in figures 4a and 4d where the **c2i0$\mathbb{E}_+^2$** set is seen from the $-s$ and $+s$ axes respectively.

In parameter space the initial point is $\overset{o}{\varphi}_0 = (0; 0, 0)$. The first iteration gives the iteration constant $\overset{o}{\varphi}_1 = \overset{o}{c} = (s; x, y)$, The second iteration for the scalar is

$$s_2 = s^2 + x^2 + y^2 + \frac{x^2 y^2}{s^2} + s \tag{3.3a}$$

and for the director components are

$$x_2 = 2x \left(s + \frac{y^2}{s} + \frac{1}{2} \right) \tag{3.3b}$$

10

$$y_2 = 2y\left(s + \frac{x^2}{s} + \frac{1}{2}\right). \tag{3.3c}$$

The x director component is an odd function of x, thus upon iteration, the function will be equal but with opposite sign under the transformation $x \to -x$. The bound criterion $\left\|\overset{o}{\varphi}\right\|^2 = \left(s^2 - x^2 - y^2 + \frac{x^2 y^2}{s^2}; 0, 0\right)$ is even under inversion of any of the axes. Therefore, the confined set and the escape velocity iso-surfaces must be symmetric about the ordinate axis. An equivalent reasoning leads to $y \to -y$ symmetry about the abscissas. The symmetry between the upper and lower half in figure 4 exhibits this $\pm y$ symmetry. Renderings of rotations about the s axis (not shown here) also confirm the $\pm x$ symmetry. The bound set is asymmetrical with respect to the scalar (or real) s axis. Indeed, from the above expression, the transformation $s \to -s$ does not have a well defined parity for the resultant scalar term $s^2 + x^2 + y^2 + \frac{x^2 y^2}{s^2} + s$. Thus, the iterated map will not be equal under inversion of the scalar axis.

3.1. Divergent magnitude surface in the vicinity of periodic points

Due to s terms in the denominators, all three components in iteration (3.3a)-(3.3c) become large for nonzero director components if the scalar becomes small. In a first approximation, allow for x, y to be small in the scalar component second iteration s_2, so that the term $\frac{x^2 y^2}{s^2}$ can be neglected; Impose the condition $s_2 \to 0$, so that the scalar term will produce a very large scator in the third iteration. The equation for s_2 in terms of the initial values is approximately $s^2 + x^2 + y^2 + s = 0$. Notice that the s terms can be collected as $s^2 + s = \left(s + \frac{1}{2}\right)^2 - \frac{1}{4}$. The equation is then $\left(s + \frac{1}{2}\right)^2 + x^2 + y^2 = \frac{1}{4}$, that is a sphere of radius $\frac{1}{2}$ centered at $\left(-\frac{1}{2}; 0, 0\right)$. This sphere crosses the scalar axis at 0 and -1. Therefore, we expect to have an unbounded region in the vicinity of $s = -1$, as it is indeed observed in figure 3. Nonetheless, there is a period two fixed point at -1 with its concomitant basin of attraction. So there is an attractive point surrounded by divergent points on a plane. The surface generated by the second iteration without approximations is $s^2 + x^2 + y^2 + \frac{x^2 y^2}{s^2} + s = 0$, it is a slightly deformed sphere as shown in figure 5. This refinement does not alter significantly the argument that has been presented. We previously found a set of large magnitude points $\mathbf{R}_s$ in the vicinity of $s = 0$. We have now found that there is also a divergent magnitude surface crossing the s axis at $s = -1$. Let us generalize this result.

Lemma 1. *For every periodic point $P^{\circ n}$ on the scalar axis, there is a divergent vicinity*
$$\mathbf{R}_{s_n} = \left\{(s; x, y) \in \mathbb{E}_+^2 : x_n \neq 0, y_n \neq 0, s_n \to 0\right\}.$$

Proof. A divergent magnitude is obtained when the scalar component of the nth iteration scator is zero, that is, $s_n = \frac{1}{2}\left(\overset{o}{\varphi}_n + \overset{o}{\varphi}_n^*\right) = 0$. Thus $\left\|\overset{o}{\varphi}_n\right\| =$

(a) 3D rendering

(b) Constant y curves for $y = 0$ (circle radius $1/2$ centered at $-1/2$), $y = 0.1, 0.2, 0.3, 0.4$ and 0.4987 (tiny curve centered at $-1/2$)
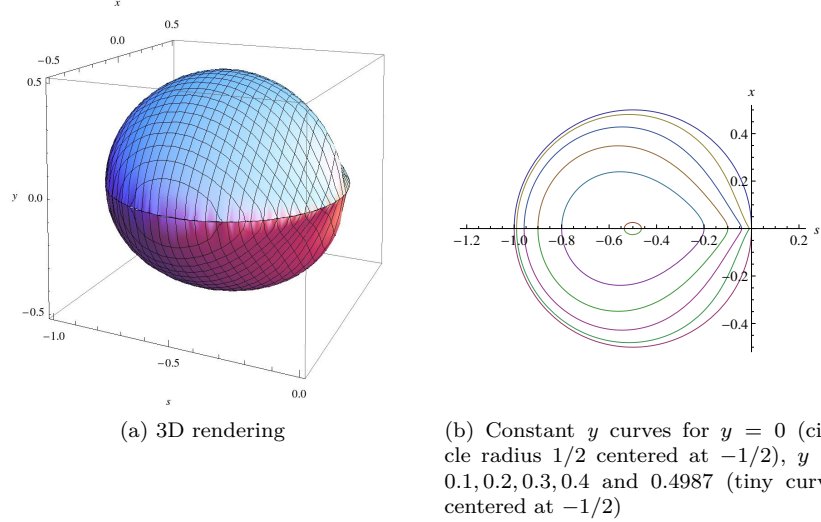
Figure 5: Plot of equation $s^2 + x^2 + y^2 + \frac{x^2 y^2}{s^2} + s = 0$. Along this surface, the scalar component in the second iteration is zero $s_2 = 0$. The scator magnitude diverges on this surface except at the planes $x = 0$ and $y = 0$. There is a period 2 point at $(-1; 0, 0)$ and the fixed point at the origin.

$s_n^2 - x_n^2 - y_n^2 + \frac{x_n^2 y_n^2}{s_n^2} \to \infty$ if $s_n(s, x, y) \to 0$ with $x_n, y_n \neq 0$. Notice that if the director components are not zero after n iterations, they are necessarily non zero for the initial constant value $\overset{o}{c} = (s; x, y)$, that is $x_n, y_n \neq 0 \Rightarrow x, y \neq 0$. Periodic points require that $\overset{o}{\varphi}_n = 0$, that is, the point represented by the scator $\overset{o}{\varphi}$ returns to zero after n iterations. Since x, y are zero on the scalar axis, $\overset{o}{\varphi}_n = (s_n; 0, 0) = 0$. But a scator with zero director components is equal to a scalar, i.e. $(s_n; 0, 0) = s_n$. Furthermore, on the scalar axis, s_n is only a function of s, namely $s_n(s, 0, 0) = 0$. But this periodic point condition on the scalar axis is equal to the divergent magnitude condition if $x_n = y_n = 0$. Thus the divergent magnitude surface has a periodic point whenever it intersects the scalar axis. □

The iterations on the scalar or real axis commence with the constant $\overset{o}{c} = (s; 0, 0)$. From (2.4a)-(2.4c), the square of a scator with zero director components is a scator whose only non-vanishing component is again the scalar component. Recall also, that addition is defined component-wise. Thus the iteration of a scalar quantity remains a scalar. In this particular case, the zeros in the director components $(s; 0, 0)$ can be dropped and only the real number s need be written down. The real roots of the corresponding polynomials establish the periodic points after n iterations, see table 1 for the first few roots. There are basins of attraction in the vicinity of these attractive periodic points in the complex

12

plane. We assume without proof, that there are also basins of attraction in the real scator space. This assumption is consistent with the numerical evaluation that exhibits smaller 3D copies of the set at the roots of the polynomial in the negative real axis (see figures 2 and 3).

point period	periodic points on scalar axis $\overset{o}{\varphi}_n = 0$	real root	divergent scator magnitude $s_n = 0$
initial value	$x, y = 0$		$x, y \neq 0$
fixed	$\overset{o}{\varphi}_1 = s$	$s = 0$	$s_1 = s$
2	$\overset{o}{\varphi}_2 = s^2 + s$	$s = -1$	$s_2 = s^2 + x^2 + y^2 + \frac{x^2 y^2}{s^2} + s$
3	$\overset{o}{\varphi}_3 = \left(s^2 + s\right)^2 + s$	$s = -1.7549$	$s_3 = s_2^2 + x_2^2 + y_2^2 + \frac{x_2^2 y_2^2}{s_2^2} + s$
4	$\overset{o}{\varphi}_4 = \left(\left(s^2 + s\right)^2 + s\right)^2 + s$	$s = -1.3107$	$\vdots$

Table 1: Attractive periodic points on scalar axis and divergent magnitude surfaces due to scalar component equal to zero.

On the other hand, points in the vicinity of the divergent magnitude surface with $s_n \ll x_n, y_n$, will have a large magnitude and will fail to fulfill the upper bound criterion (3.1). Furthermore, all three components in the $n + 1$ iteration (3.2a)-(3.2c) become large for nonzero director components if the s_n scalar becomes small. Imposing the condition that the scalar component becomes zero in the nth iteration, produces a divergent result for all three components in the next iteration if $x_{n+1}, y_{n+1} \neq 0$. In contrast with what we stated before, in this case, the large magnitude condition is equivalent to the large scalar component condition.

The basin of attraction of periodic points on the scalar axis becomes squeezed in the x, y plane at the periodic point. This is indeed what is observed in figure 3. The roots at 0, -1, -1.3107 clearly exhibit a waist.

The basin of attraction of periodic orbits of maps on the real line has only recently been addressed. There are no globally attractive periodic orbits of continuous maps on connected metric spaces. In contrast, fixed points can be globally attractive [Elaydi and Sacker, 2004]. It will be interesting to attempt extending the dynamics in the neighborhood of a periodic point to higher dimensions such as three dimensional scators. In particular, the notions of attracting and repelling orbits.

The extended complex plane is homeomorphic to the two-dimensional sphere $S^2 = \left\{(x_1, x_2, x_3) \in \mathbb{R}^3 | x_1^2 + x_2^2 + x_3^2 = 1\right\}$. Infinity in $\bar{\mathbb{C}}$ is then mapped onto a single point at the sphere pole $x_3^2 = 1$. The point at infinity can then be thought as a superattractive fixed point [Blanchard, 1984]. Whether it is possible to produce a homeomorphism of $\bar{\mathbb{E}}_+^2$ with a three-dimensional sphere is an open problem. Nonetheless, the scator divergent magnitude surfaces can be thought as a superattractive surface at infinity.

13

4. Sections of the c2i0$\mathbb{E}^2_+$ set in the s, x plane

4.1. Quadratic iteration with hyperbolic numbers

In 1+1 dimensions, positive or real scator algebra becomes identical to hyperbolic numbers algebra $\mathbb{H}$ as may be readily seen from the product definition (2.1a)-(2.1c) with any of the two director components with subindex 1 or 2 equal to zero. Furthermore, distributivity of the product over addition is recovered. Since hyperbolic numbers are equivalent to scators with only one director component $\mathbb{H} \to \mathbb{E}^1_+$, the sets **c2i0$\mathbb{H}$** and **c2i0$\mathbb{E}^1_+$** are equal. The quadratic iteration with hyperbolic numbers gives rise to a square centered at $-\frac{7}{8}$ with sides equal to $\frac{9}{4\sqrt{2}}$ [Senn, 1990]. The square diagonals (with $\frac{9}{4}$ length) lie parallel to the real and hypercomplex axes. If the bound criterion for a hyperbolic number $a + b\,\hat{\mathbf{e}}$, $(\hat{\mathbf{e}} \cdot \hat{\mathbf{e}} = 1, \ \hat{\mathbf{e}} \notin \mathbb{R})$ is $a^2 \leq \varepsilon$ and $b^2 \leq \varepsilon$, the bound set is equal to a square [Metzler, 1994]. This set is the counterpart of the Mandelbrot set for complex numbers but in two dimensional hyperbolic geometry [Artzy, 1992]. The boundary for the hyperbolic set, is made up of four straight lines void of the complexity shown by the M-set. There are neither small-copies of the set nor a structure within the bound region as can be seen in the first inset of figure 6. Thus, the rich fractal 3D structure is lost when it is projected into 2D.

The iteration on the real positive axis is bound from 0 to 1/4. The iteration on the director axes for $s = 0$ is then also bound from 0 to 1/4 since the sides of the square bound set are rotated at $\pi/4$. Since the mapping is symmetric with respect to the director axes it must be bound from $-1/4$ to 1/4. A similar argument follows for the other director axis. So the points located within a cross centered at the origin of the x, y plane at $s = 0$ with 1/4 length per arm produce bound iterations. The quadratic iterated function of any other point in the $s = 0$ plane diverges as shown in figure 1.

4.2. The s, x plane

A rich fractal like structure is revealed if the second director component is set to small value different from zero. Evaluation at hypercomplex plane $y = 10^{-20}$ already exhibits a complex structure [Fernández-Guasti, 2013, submitted]. In a sequence, depicted in figure 6, we show sets from **c2i0$\mathbb{E}^2_+$**$(s; x, 0)$ to **c2i0$\mathbb{E}^2_+$**$(s; y, 0.8)$ in steps of $\triangle y = 0.1$. Points are evaluated starting at $\overset{o}{\varphi}_0 = (0; 0, 0)$ and $\overset{o}{c} = (s; x, y)$, s is scanned in the ± 2.0 interval centered at -1.0 while x is centered at 0. The bounded region becomes smaller and departs form the diamond-like shape moving towards a bird-like form as the y hyperplane is increased. The set is always squeezed in the forefront to the right in the plane where $s = 0$ if $y \neq 0$. Furthermore, the escape velocity in the $s = 0$ plane is very large (lighter blue) as may be seen in the insets of figure 6. This plane is enlarged as the y plane is further away from the origin. This is the expected behaviour due to the large magnitude set $\mathbf{R}_s$ described in (2.6) encountered in the vicinity of the $s = 0$ plane. A large escape velocity (light blue) circle with
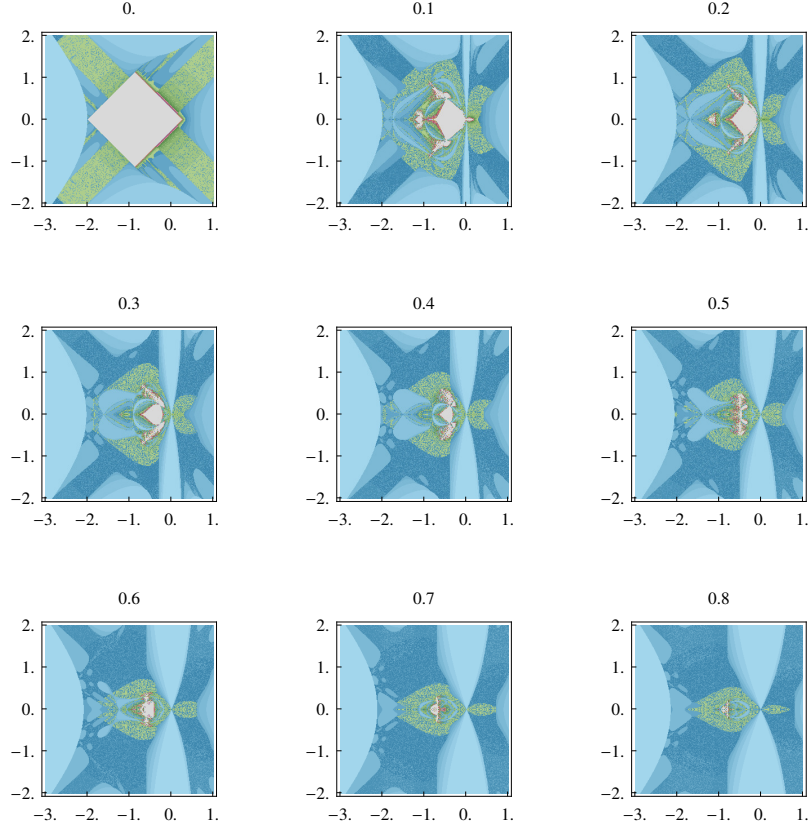
14

Figure 6: Slices of the bound quadratic iteration $\mathbf{c2i0}\mathbb{E}_+^2(s; x, y)$ set with y hyper-axis between 0 and 0.8 in 0.1 steps. The abscissa s is scanned in the ± 2.0 interval centered at -1.0 whereas the ordinate x is scanned in the same interval but centered at the origin.

radius approximately $1/2$ centered around $s = -1/2$ can be clearly seen in the insets $y = 0.1$ and 0.2 of figure 6. These large iso-escape velocities correspond to the second iteration divergent magnitude surface. The level curves plotted in figure (5b) can be followed in the insets 0.1 to 0.4 of figure 6. At $y = 0.5$, the second iteration divergent magnitude surface just touches the plane at only one point and is no longer present for $y > 0.5$.

So far, we have described squeezing of the set at the periodic points on the scalar axis. The $\mathbf{R}_{s_2}$ surface also prevents points to be bounded off axis. The bound set is squeezed when it meets the rim of the $\mathbf{R}_{s_2}$ surface. See for example the thin attachment of the wings to the main body in insets 0.1 to 0.4 of figure 6. The $\mathbf{R}_{s_2}$ surface repels points that approach it, since the $n + 1$ iteration will have very large values for all three components.

The $s_3 = 0$ polynomial is already rather lengthy to write down in terms of the initial $\overset{o}{c} = (s; x, y)$ values. Its roots are analytically solvable although they are even lengthier. However, the intersection of this surface with the $y = 0$ plane is quite tractable. From table (1),

$$s_3 = s_2^2 + x_2^2 + s,$$

because $y = 0 \Rightarrow y_2 = 0$. Substitution of s_2 and x_2 from (3.3a) and (3.3b) respectively gives

$$s_3 = \left(s^2 + x^2 + s\right)^2 + 4x^2 \left(s + \frac{1}{2}\right)^2 + s = 0.$$

The real solutions for x are

$$x = \pm \frac{\sqrt{\sqrt{32s^4 + 64s^3 + 44s^2 + 8s + 1} - \left(6s^2 + 6s + 1\right)}}{\sqrt{2}},$$

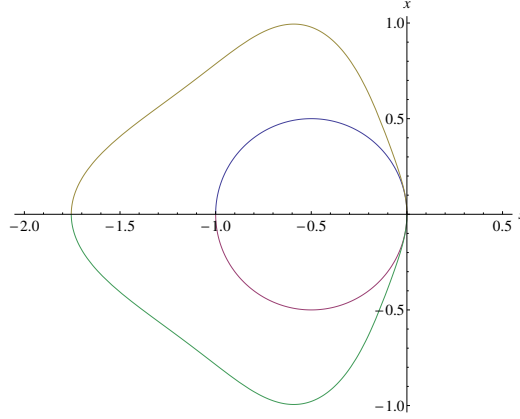this function is plotted in figure 7. The magnitude squared for a scator in the

Figure 7: Intersection of the $s_3 = 0$ and $s_2 = 0$ (circle) surfaces with the $y = 0$ plane.

third iteration is

$$\left\|\overset{o}{\varphi}_3\right\|^2 = s_3^2 - x_3^2 - y_3^2 + \frac{x_3^2 y_3^2}{s_3^2}.$$

Since $y = 0 \Rightarrow y_3 = 0$, then $\left\|\overset{o}{\varphi}_3\right\|^2 = s_3^2 - x_3^2$ and for points on the intersection with the surface $s_3 = 0$

$$\left\|\overset{o}{\varphi}_3\right\|^2 = -x_3^2 = -\left(2s_2 x_2 + x\right)^2 = -\left(2x\left(s^2 + x^2 + s\right)\left(2s + 1\right) + x\right)^2,$$

where we have used the iteration relationship (3.2b). This magnitude is certainly finite in the interval ± 2 in either variable. However, as soon as $y \neq 0$, the

16

magnitude becomes divergent. The curve shape is not altered significantly for very small values of y. Just as in the $s_2 = 0$ condition, small departures from $y = 0$ yield similar curves, as observed in figure 5b. There is a high escape velocity (light blue) contour of the form given by the $s_3 = 0$ polynomial (depicted in figure 7) in inset 0.1 of figure 6. Again, at approximately $s = -0.9, x = \pm 0.9$ the confined set is squeezed due to the presence of the third iteration divergent magnitude surface.

The out-most bound point must be located at $y = \frac{9}{8} = 1.125$ where the upper tip of the diamond is located. Recall that there must be a diamond-like shape in the perpendicular s, y plane identical to the one shown in the first s, x inset. This feature is no longer visible even at smaller values of the y planes because the tip becomes very thin and is difficult to see at this magnification. From previous estimates [Fernández-Guasti, 2013], the tip is approximately 10^{-7} thick between 1.0 and 1.125.

5. Conclusions

The quadratic iteration in three dimensional real scator space $\mathbb{E}_+^2$ exhibits a rich boundary structure with complex dynamics. The extended set including points at infinity $\bar{\mathbb{E}}_+^2$ has been introduced. This set, beside the usual points whose components tend to infinity, also contains scator elements with null scalar and finite director components. That is, the scator norm contains a plane $\mathbf{R}_s$ where the magnitude diverges. The $\mathbb{E}_+^2$ scator algebra is not distributive and contains divisors of zero as well as non-invertible elements. The algebra forms a commutative group if divisors of zero and non invertible elements are excluded. The confined iteration notation $\mathbf{c2i0}\mathbb{E}_+^2(s; x, y)$ seems at present rather clumsy. However, we believe that it will prove very useful as the scator set is extended to higher dimensions and diverse mappings. The $\mathbf{c2i0}\mathbb{E}_+^2(s; x, y)$ set has been defined in parameter space in terms of bounded iterations. Some features of the 3D set have been described, such as the self similarity of the elementary fractal as well as elementary fractal components. The position of self similar smaller copies has been discussed elsewhere [Fernández-Guasti, 2013]. The main set spatial symmetries have been discussed. The existence of divergent magnitude surfaces in the vicinity of periodic points on the scalar axis has been proved. Squeezing of the set at the divergent magnitude surfaces has been noted, both on and off the scalar axis. Flat images of the three dimensional rendering of this set have been rendered with the open source program developed by P. Willenius [Willenius, 2013]. We have shown that increasing the number of iterations gives a closer fidelity to the actual set boundary but some features are lost. In particular very thin surfaces are no longer rendered. A possibility in order to visualize these features is to have a variable thickness evaluation mesh and to introduce transparency for very thin features. New algorithms will certainly be required to visualize the intricacies of these higher dimensional sets. Two dimensional renderings also prove useful to understand the dynamics. In

particular, they have been utile here in order to assess escape velocities that are related to the $\mathbf{R}_{s_n}$ divergent magnitude surfaces.

Acknowledgements

References

J. Aron. The Mandelbulb: first 'true' 3D image of famous fractal. *New Scientist*, Nov 2009.

R. Artzy. Dynamics of quadratic functions in cycle planes. *Jour. Geometry*, 44: 26–32, 1992. URL `http://double.numbers/artzy-jg1992.pdf`.

J.M. Blackledge. *Fractal Geometry: Mathematical Methods, Algorithms, Applications*. Woodhead Publishing, 2002. ISBN 978-1904275008.

P. Blanchard. Complex analytical dynamics on the Riemann sphere. *Am. Math. Soc.*, 11(1):85–141, 1984.

M. Dodge, M. McDerby, and M. J. Turner, editors. *Geographic Visualization: Concepts, Tools and Applications* . Wiley-Blackwell, 2008. ISBN 978-0470515112.

A. Douady and J. H. Hubbard. Exploring the Mandelbrot set, 1984.

S. Elaydi and R. Sacker. Basin of Attraction of Periodic Orbits of Maps on the Real Line. *Journal of Difference Equations and Applications*, 10(10):881–888, 2004. doi: 10.1080/10236190410001731443. URL `http://www.tandfonline.com/doi/abs/10.1080/10236190410001731443`.

M. Fernández-Guasti. Lagrange's identity obtained from product identity. *Int. Math. Forum*, 7(52):2555–2559, 2012. ISSN 1312-7594. URL `http://www.m-hikari.com/imf/imf-2012/49-52-2012/fernandezguastiIMF49-52-2012.pdf`; `http://lagid-complex2.lyx`.

M. Fernández-Guasti. Fractals with hyperbolic scators in 1+2 dimensions. *Fractals*, 2013. ISSN 0218-348X, 1793-6543. submitted: FRACTALS-D-12-00044.

M. Fernández-Guasti and F. Zaldivar. A hyperbolic non distributive algebra in 1+2 dimensions. *Adv. Appl. Clifford Algebras*, 2013. ISSN 0188-7009, 1661-4909. in print.

J. Leys. Sphere inversion fractals. *Computers & Graphics*, 29(3): 463–466, 2005. ISSN 0097-8493. doi: 10.1016/j.cag.2005.03.011. URL `http://www.sciencedirect.com/science/article/pii/S0097849305000531`.

W. Metzler. The "mystery" of the quadratic Mandelbrot set. *Am. J. Phys.*, 62 (9):813–814, 1994. URL `http://double.numbers/metzler-ajp1994`.

D. G. Pavlov, Panchelyuga M. S., Malykhin V. A., and Panchelyuga V. A. On fractality of Mandelbrot and Julia sets on double-numbers plane. *Hypercomplex numbers in geometry and physics*, 6:135–145, 2009.

P. Senn. The Mandelbrot set for binary numbers. *Am. J. Phys.*, 58(10):1018, 1990. URL `http://double.numbers/senn-ajp1990`.

P. Willenius. Fractrace. *https://github.com/trafassel/Gestaltlupe*, 2013.